Check for updates

View Article Online
View Journal

Journal of
Materials Chemistry A
Materials for energy and sustainability

Accepted Manuscript

This article can be cited before page numbers have been issued, to do this please use: C. Zha, X. Chen, Y. Zhao, K. S. Hui, L. Zhang, Y. Zheng, H. Xu, Q. Jiang, K. N. Hui and T. Chen, *J. Mater. Chem. A*, 2024, DOI: 10.1039/D4TA02558J.

Volume 6
Number 12
28 March 2018
Pages 4883-5230

Journal of
Materials Chemistry A
Materials for energy and sustainability
rsc.li/materials-a

ISSN 2050-7488

ROYAL SOCIETY
OF CHEMISTRY

COMMUNICATION
Zhenhai Wen *et al.*
An electrochemically neutralized energy-assisted low-cost acid-alkaline electrolyzer for energy-saving electrolysis hydrogen generation

This is an Accepted Manuscript, which has been through the Royal Society of Chemistry peer review process and has been accepted for publication.

Accepted Manuscripts are published online shortly after acceptance, before technical editing, formatting and proof reading. Using this free service, authors can make their results available to the community, in citable form, before we publish the edited article. We will replace this Accepted Manuscript with the edited and formatted Advance Article as soon as it is available.

You can find more information about Accepted Manuscripts in the Information for Authors.

Please note that technical editing may introduce minor changes to the text and/or graphics, which may alter content. The journal's standard Terms & Conditions and the Ethical guidelines still apply. In no event shall the Royal Society of Chemistry be held responsible for any errors or omissions in this Accepted Manuscript or any consequences arising from the use of any information it contains.

ROYAL SOCIETY
OF CHEMISTRY

rsc.li/materials-a

View Article Online
DOI: 10.1039/D4TA02558J

Commercially Available Ionic Liquids Enables High-Performance of Aqueous Zinc-Iodine Batteries: Sequestered Nitrogen-sites for Efficient Electrocatalytic Iodine Conversion

Xinyu Chen,[a,+] Yuwei Zhao,[a,+] Yunshan Zheng,[b] Huifang Xu,[b] Qingbin Jiang,[b] Tianyu Chen,[b] Kwan San Hui,[d] Kwun Nam Hui,[b,*] Linghai Zhang,[a,*] Chenyang Zha,[a,b,c,*]

[a] Key Laboratory of Flexible Electronics (KLOFE), School of Flexible Electronics (Future Technologies), Institute of Advanced Materials (IAM), Nanjing Tech University, Nanjing, 211816, China

[b] Institute of Applied Physics and Materials Engineering (IAPME), Zhuhai UM Science & Technology Research Institute (ZUMRI), University of Macau, Taipa, 999078, Macau SAR, China

[c] Guangdong-Hong Kong Joint Laboratory for Carbon Neutrality, Jiangmen Laboratory of Carbon Science and Technology, Hong Kong University of Science and Technology (Guangzhou), Jiangmen, 529199, China

[d] School of Engineering, Faculty of Science, University of East Anglia, Norwich, NR4 7TJ, United Kingdom

+ These authors contribute equally to this article.

* Corresponding author e-mail:
bizhui@um.edu.mo (K. Hui);
iam.lzhang@njtech.edu.cn (L. Zhang);
chenyangzha@um.edu.mo (C. Zha)

View Article Online
DOI: 10.1039/D4TA02558J

Abstract

The high performance of aqueous zinc-iodine batteries is limited by the soluble polyiodide shuttling and sluggish redox kinetics. Various strategies have been proposed to address these issues, but most of these optimizing strategies either add additional hurdles to the manufacturing process or require materials that are not currently commercially available. Herein, we take advantage of commercial 1,2-dimethyl-3-propylimidazolium iodide to serve as a redox reaction catalyst for the activation of iodine cathodes without any other material modification. Due to the strong bonding coordination between 1,2-dimethyl-3-propylimidazolium iodide and the polyiodides, the as-prepared cell has a high specific capacity (147 mAh/g) at 50 C, and ultralong cycling performance (20000 cycles) with better capacity retention. This work introduces an effective and commercial material that enables bringing aqueous rechargeable zinc iodine batteries to the practical energy market.

View Article Online
DOI: 10.1039/D4TA02558J

Introduction

Aqueous zinc batteries have emerged as highly attractive energy storage candidates due to their confluence of desirable features,[1-7] which are abundant and inexpensive metallic zinc resources, low fabrication costs, and favorable electrochemical properties.[2, 8-13] Among various cathode materials of zinc batteries, iodine offers a compelling combination of properties for rechargeable zinc-iodine battery (Zn-I_2), which boasts a high theoretical specific capacity of 211 mAh/g, a favorable discharge potential plateau of 1.38 V versus Zn/Zn^{2+}, and readily available resources with estimated concentrations of 55 μg/L in seawater.[10-12, 14]

Despite their promise for aqueous energy storage,[15-18] current Zn-I_2 batteries face several significant challenges. On the anode side, zinc metal suffers from both dendrite growth and thermodynamically favored hydrogen evolution reaction.[19-21] At the cathode, high concentrations of polyiodide intermediate compounds are generated during the electrochemical redox reaction of iodines, and this leads to detrimental "shuttle" effects.[11, 12] These shuttling effects cause irreversible loss of active materials, corrosion, and consumption of the zinc anode. The use of electrocatalysts to accelerate the iodine reaction kinetics and regulate the zinc dendrite growth has shown promise,[14] which is attractive due to its ease of implementation and cost-effectiveness. Especially, the intrinsically weak van der Waals interactions holding iodine molecules together within their crystalline structure pose a significant challenge for the practical implementation of iodine-based batteries.[19, 20, 22] These weak forces facilitate spontaneous sublimation and compromise the thermal stability of iodine under ambient conditions. This translates to a gradual loss of active material of cathodes, leading to capacity fade and diminished cycle life in full batteries. Addressing this fundamental limitation through material design modifications or structural engineering will be crucial for unlocking the full potential of iodine-based energy storage systems.[23-25] Extensive research has explored various electrolyte modifications, such as incorporating additives, increasing electrolyte concentration, employing polymer gel electrolytes, and inducing the functional N atoms of molecules.[9, 15] Those electrolyte optimizations show the potential of carefully selected electrolyte additives to simultaneously interact with iodine species and mitigate key side reactions in zinc-iodine batteries,[26-28] which opens exciting avenues for further exploration of nitrogen-containing molecular and functional nitrogen sites of the interface as promising additives to optimize Zn-I_2 battery performance.[9, 16, 17, 29] While certain electrolyte

View Article Online
DOI: 10.1039/D4TA02558J

formulations have demonstrated improvements in electrochemical performance, these advancements often come at the expense of economic viability. Notably, the solid/quasi-solid and concentrated electrolytes employed in these cases significantly inflate material costs compared to conventional dilute aqueous electrolytes. This discrepancy necessitates further investigation into optimizing performance within cost-effective constraints, a crucial step for the translation of high-performing Zn-I_2 batteries.[10-12, 20, 21]

Despite ongoing efforts to address the drawbacks of Zn-I_2 batteries, translating laboratory advancements into practical applications confronts significant hurdles.[9, 13, 17] Existing mitigation strategies often face scalability challenges of material preparation, with intricate manufacturing processes escalating fabrication costs and complexity. Moreover, dependence on materials lacking commercial availability introduces uncertainties regarding long-term supply and cost competitiveness. Consequently, the critical path forward lies in the development of cost-effective and commercially available strategies-based materials that leverage readily available materials and integrate seamlessly with existing production lines.[16, 17, 30] It is, therefore, attractive to develop a strategy allowing the usage of commercially available electrocatalytic materials, which can possess high electrical conductivity to compensate the electrons for electrochemical reactions in addition to the catalytic activity.[26-28]

In this work, the commercialized 1,2-dimethyl-3-propylimidazolium iodide (DMPII) with activated N sites of multiple-functional properties are proposed as the catholyte additive, offering stable electrochemical reactions in aqueous Zn-I_2 batteries. As prepared DMPII-based Zn-I_2 cells show the effective restrain the undesired shuttle effect, in which long-chain organic matrix with the N-sites offer physical confinement by the van der Waals forces and steric hindrance, and chemical interactions by the N-I bonds of polyiodide anions. More importantly, the congruent molecular orbitals of DMPII hinder the coordination reaction between I_3^- and I^- by competitive adsorption, suppress the shuttling effect, and attribute to a high Coulombic efficiency. As a result, the DMPII-based Zn-I_2 cell exhibits a stable specific capacity of 147 mAh/g and 99 % Coulombic efficiency at 50 C (10 A/g), and reaches a 70 % capacity retention rate following 20000 cycles. The presented strategy for designing electrodes utilizes commercially available materials, which alignment with existing manufacturing infrastructure and readily available resources hold immense potential for accelerating the development and commercialization of high-performance Zn-I_2 batteries.

View Article Online
DOI: 10.1039/D4TA02558J

Results and Discussion

The unique structural and electronic properties of 1,3-dimethyl-2-phosphinoimidazole (DMPII) hold promise for mitigating polyiodide shuttling, a major bottleneck in Zn-I_2 batteries. As depicted in Fig. 1, the iodophilic N sites within DMPII generate sufficient polarity to capture polyiodides within the cell, while its well-suited molecular orbitals facilitate rapid electron transport. This combination promotes efficient polyiodide conversion and enhances iodine utilization, leading to superior performance compared to conventional I_2 cathodes where polyiodide shuttling to the zinc anode compromises Coulombic efficiency and cycling stability.[11, 12, 24] To elucidate the impact of DMPII on LiI+I_2 cathode crystallization, X-ray diffraction (XRD) analysis is conducted (Fig. 2a-b). The peaks at approximately 24° and 29° correspond to the (111) (200) and (121) planes of standard iodine material (JCPDS No. 35-1385), respectively.[31] Notably, the (200) peak intensity significantly increases for DMPII-modified cathodes, signifying enhanced crystallinity and potentially a more stable interface. Furthermore, a slight shift in the diffraction peak towards higher angles (Fig. 2b) suggests modulation of the crystal lattice spacing by DMPII.[19, 32] This enlarged interlayer within the DMPII/LiI+I_2 composite likely offers two crucial advantages: improved ionic conductivity for enhanced electrotransport and simultaneous polyiodide immobilization, ultimately leading to an accelerated conversion process and promising performance improvements.[14-16] To further probe the interfacial influence of DMPII on the cathode interface of LiI+I_2, scanning electron microscopy (SEM) and atomic force microscopy (AFM) are employed to analyze the cathode films. The SEM image of the pure LiI+I_2 cathode reveals a rough morphology with small grains, likely arising from the fast crystallization rate and anisotropic crystallization direction (Fig. 2c). With the introduction of DMPII, the cathode film shows a smooth interface with a more compact morphology (Fig. 2e). This can be attributed to the slowed crystal growth rate of LiI+I_2 cathode films induced by the Lewis acid-base interaction between DMPII and LiI+I_2.[27-29] The corresponding AFM images (Fig. 2d and f) suggest that the addition of DMPII can greatly decrease the surface roughness of LiI+I_2 films, which changes from 2 to 0.6 μm. High-quality cathode films can enhance the electrochemical reaction kinetics and benefit interfacial charge transfer.[23, 24, 33]

The electrochemical kinetics is further investigated through the cyclic

View Article Online
DOI: 10.1039/D4TA02558J

voltammetry (CV) curves of Zn-I_2 cells in the voltage range of 0.6-1.6 V (Fig. 3a), which expands significantly after adding DMPII to the LiI+I_2 catholyte (DMPII/LiI+I_2). The corresponding pairs of redox peaks (approximately 1.4 and 1.3 V) in the aqueous electrolyte are indexed to the I_2/I^- processes during the cycles.[14, 34, 35] The shifting reversible redox peak with the largest area is related to the enhanced electrochemical reactivity of the battery with the DMPII activator, where the obvious potential difference between the redox peaks suggests the exceptional reversibility of zinc plating/stripping coupled with a rapid iodine conversion process.[16, 17, 36, 37] This efficient electrochemical reaction kinetics can be ascribed to the dominant activated N sites of molecules arising from the fast reaction kinetics facilitated by DMPII. To elucidate the effect of DMPII on reaction kinetics and catalytic activity, Tafel slopes are extracted from the corresponding CV curves (Fig. 3b-c).[16, 23, 35] Strikingly, DMPII-modified LiI+I_2 electrodes exhibit significantly lower Tafel slopes of 130 and 112 mV/dec for the reduction and oxidation processes, respectively, compared to 190 and 226 mV/dec observed for the pure LiI+I_2 electrode.[11, 12] This remarkable decrease signifies substantially enhanced electrocatalytic activity and much faster kinetic processes within the DMPII-activated Zn-I_2 battery system. Meanwhile, the corresponding current of redox peaks is higher than that of the pure LiI+I_2 electrode (Fig. 3d), which exhibits better electrochemical reaction kinetics and iodine utilization in the DMPII-modified LiI+I_2 catholyte.[9, 31] Then, electrochemical impedance spectroscopy (EIS) is used to analyze the resistance of the electrode interface. The Nyquist plots (Fig. 3e) of the DMPII-modified LiI+I_2 cell show much smaller interface resistance than that of the pure LiI+I_2 electrolyte.[8, 23, 24, 38] This remarkable decrease suggests that DMPII effectively enhances ionic conductivity and diffusion coefficient, further confirming the advantageous effect of the activated N sites in boosting the performance of the iodine redox reaction.[36, 38, 39] Furthermore, the CV is performed at both constant and rated scan rates to comprehensively assess the electrocatalytic activity of DMPII-modified LiI+I_2 catholyte. At a scan rate of 0.8 mV/s (Fig. 3f), the nearly overlapping redox potential curves (Fig. 3g) demonstrate minimal polarization during the polyiodide reaction, highlighting efficient redox kinetics and rapid electron transfer. Increasing the scan rate from 0.4 to 1.0 mV/s (Fig. 3h) reveals a linear relationship between peak current density (I_A and I_C) and the square root of the scan rate (Fig. 3i), suggesting highly ordered Zn^{2+} diffusion. These combined results showcase the

View Article Online
DOI: 10.1039/D4TA02558J

profound impact of DMPII: efficient facilitation of polyiodide redox kinetics and enhanced Zn^{2+} transport within the electrolyte system.[8, 40]

To elucidate the fundamental role of DMPII in polyiodide redox reactions, monitoring the absorbance of I^- solutions (approximately 3.0 x 10^{-3} mol/L of I^-), and Ultraviolet-visible (UV-vis) spectroscopy are employed to investigate the anchoring capability of DMPII-modified $LiI+I_2$ electrodes, where the current collector is carbon paper (CP). After 20 h, the absorbance of I^- solutions progressively diminishes, transitioning from an initial detectable state to complete transparency (Fig. 4a). This dramatic decrease suggests efficient anchoring and immobilization of I_3^- on the current collector by DMPII. Further corroborating this, the characteristic I_3^- UV-vis peaks at approximately 285 and 350 nm steadily decline in intensity (Fig. 4b).[22] These combined observations provide compelling evidence for the exceptional performance of DMPII-activated $LiI+I_2$ electrodes, likely arising from highly reversible electrochemical reactions facilitated by DMPII.[10, 11] Chronoamperometry reveals the superior performance of the DMPII-modified $LiI+I_2$ cell compared to its unmodified counterpart (Fig. 4c). The DMPII-modified cell consistently maintains a higher current response, highlighting its enhanced electrocatalytic activity. Further elucidating the underlying mechanism, Cottrell plots unveil diffusion limitations at the electrode interface during the redox process. Notably, the current response estimates from Cottrell polts, which is significantly higher for the DMPII-modified cell (30 mA/cm² versus 16 mA/cm² for the unmodified cell), indicating accelerated mass transport of iodine species facilitated by DMPII.[41] Next, the CV curves are performed on symmetrical cells (Fig. 4d). the DMPII/$LiI+I_2$ electrode exhibits significantly higher current responses compared to the pure $LiI+I_2$ electrode, demonstrating its superior electrochemical activity during polyiodide redox reactions. These observations provide strong evidence for the beneficial role of DMPII in facilitating electron transfer. To delve deeper into the reaction kinetics, Tafel plots are constructed based on the redox peaks observed in the CV curves (Fig. 4e-f). In the oxidation process, the Tafel slopes for DMPII/$LiI+I_2$ and pure $LiI+I_2$ electrodes are estimated at 193 and 340 mV/dec (Fig. 4e), respectively. Similarly, for the reduction peak, the corresponding values are 101 and 342 mV/dec (Fig. 4f), respectively.[9, 15] More importantly, the slower slopes reveal the DMPII-modified electrode signifies faster reaction kinetics, highlighting its catalytic prowess. This enhanced performance can be attributed to the functional active N sites within

View Article Online
DOI: 10.1039/D4TA02558J

DMPII, further supporting its role as a potent activator for polyiodide redox reactions.[9, 15] *In situ* Raman spectroscopy unveils complete polyiodide conversion in the Zn-I_2 cells: To directly observe the dynamic changing/discharging during cell operation, *in situ* Raman spectroscopy detect DMPII-modified DMPII/LiI+I_2 and pure LiI+I_2 cathodes in Zn-I_2 batteries. The corresponding DMPII-modified cathode exhibits a fundamentally efficient polyiodide conversion pathway compared to its unmodified counterpart. During charge in the DMPII-modified cell, the intensity of the characteristic I_3^- peak at approximately 110-120 cm^{-1} steadily increases (Fig. 4g), indicating the intermediate formation of this species. The DMPII-modified cathode showcases complete conversion, where the I_3^- peak progressively weakens in the later stages of charge and ultimately disappears entirely, signifying full transformation into lower-order iodide species. This complete conversion is mirrored during discharging, with the I_3^- peak reappearing and then vanishing again. Importantly, this disappearance following charge and discharge confirms the entire cycle path in the DMPII-modified cell. In stark contrast, the pure LiI+I_2 cathode exhibits incomplete conversion in the Zn-I_2 battery. The I_3^- peak remains prominent throughout both discharge and charge (Fig. 4h), revealing persistent intermediate accumulation. This dominance of I_3^- prevents complete utilization of the active species, leading to gradual capacity fade and ultimately shorter cycle life for the Zn-I_2 battery with the unmodified cathode.[11, 15, 19]

The impact of DMPII on performance is strikingly evident in cycling tests. First of all, the cycle performances of DMPII with other concentrations show capacities of approximately 93, 104, and 87 mAh/g, and retain approximately 88, 95, and 80 mAh/g after 50 cycles under the 5 A/g, which is 0.4, 0.6, and 0.8 M DMPII, respectively (Fig. S1a). The corresponding galvanostatic charge/discharge profiles show that both Zn-I_2 batteries exhibit a typical charge/discharge platform at a current of 25 C, where the potential difference (ΔV) between the oxidation and reduction plateaus at 50 mAh/g of capacity is indicative of the polarization associated with the redox reaction (Fig. S1b). Comparing the different DMPII contents (Fig. S1c), 0.6 M DMPII cell exhibits the lowest polarization potential of approximately 0.138 V, which was significantly lower than those of both 0.4 and 0.8 M DMPII cell (approximately 0.168 and 0.221 V). This finding suggests that DMPII-based cells with suitable contents of DMPII can enhance the redox reaction kinetics of polyiodides. Secondly, the performance of different volumes of $ZnSO_4$ + Li_2SO_4 electrolyte are also analyzed., which is 80, 100, and 120 mL electrolyte. The performances of the different electrolyte contents-based Zn cells show capacities of approximately 96, 102, and 90 mAh/g with 1 mg/cm^2 I_2 mass loading, and retain approximately 91, 99, 85 mAh/g after 50 cycles under the 1A/g, which is 90, 100 and 120 mL of $ZnSO_4$ + Li_2SO_4 electrolyte, respectively (Fig. S2). After comparison, it appears that the influence of varying electrolyte contents on battery performance is not particularly significant, which characteristic can increase the overall energy density of the battery by reducing the electrolyte content. Next, the DMPII/LiI+I_2 cells (0.6 M DMPII) deliver impressive capacities of approximately 100 and 95 mAh/g at 0.6-1.6 V, and remarkably retain approximately 86 and 80 mAh/g after 9000 cycles at high current densities (5 and 7 A/g), corresponding to 25 and 35 C rates, respectively (Fig. 5a-b). In stark contrast, pristine LiI+I_2 cells exhibit significantly lower capacities (68 and 68 mAh/g at 5 and 7 A/g, respectively) and demonstrate faster capacity fade. Moreover, Coulombic efficiencies exceeding 99 % in DMPII-modified cells highlight their exceptional reversibility compared to the approximately 95 % achieved by pure LiI+I_2 cells. These remarkable results underscore the transformative potential of DMPII in unlocking superior cycling performance and stability for Zn-I_2 batteries. Beyond impressive capacity and cycle stability, DMPII unlocks remarkable rate performance in Zn-I_2 batteries. The DMPII/LiI+I_2 cell delivers exceptional capacities of approximately 200, 195, 185, 175, and 145 mAh/g at current densities ranging from 1 to 10 A/g (1, 2, 3, 4, and 10 A/g), effortlessly returning to 199 mAh/g upon reverting to 1 A/g (Fig. 5c). The LiI+I_2-based Zn-I_2 cell shows 125, 118, 107, 97, 72, and 118 mAh/g at the same current densities Meanwhile, this superior performance is further corroborated by the stable charge-discharge curves of the DMPII-modified cell across various rates (Fig. 5d). These remarkable observations can be attributed to DMPII's ability to accelerate conversion reactions between iodine species while mitigating solution and shuttle processes. This enhanced kinetic control results in superior electrochemical reaction kinetics and a thermodynamically favorable conversion between I_2 and I^-, ultimately leading to the observed improvements in both capacity retention and rate capability.[23-25] To definitively elucidate the role of DMPII in mitigating the detrimental shuttle effect, the self-discharge behavior of both unmodified and DMPII-modified cells is tracked. After a 12-hour rest period, the DMPII-modified cell retains an impressive 85.9 % of its initial capacity, while the unmodified cell plummets to a mere 34.3 % (Fig. 5e). This stark difference shows

View Article Online
DOI: 10.1039/D4TA02558J

DMPII's remarkable ability to suppress iodine migration within the battery, a critical factor in achieving long-term stability and improved cyclability. Distinguished cycling stability is also achieved at a higher current density of 10 A/g (50 C). The DMPII/LiI+I_2 cell delivers an initial specific capacity of 147 mAh/g, and ultralong cycling performance of over 20000 cycles is achieved with a capacity retention of 70 % (Fig. 5f), where the corresponding charge and discharge curves show the characteristics of typical redox process of iodine (Fig. 5g). More importantly, there is no significant difference in polarization voltage of DMPII/LiI+I_2 cell (Fig. 5h). By comparison with some representative reports in the literature, the DMPII/LiI+I_2 battery delivers an outstanding cycling life and competitive capacity (Fig. 5i). These results indicate that the strong structure confinement of polyiodide in DMPII materials enables a high-performance and long-life Zn-I_2 battery.

The structural evolution of Zn anodes in DMPII is investigated by multiple characterizations. The scanning electron microscopy (SEM) is used to monitor the morphology of the charged zinc anodes, and the SEM image of pure Zn represents a comparison (Fig. S3a). In zinc cells, the electrode often exhibits randomly oriented plate-like zinc deposits. This irregular deposition behavior promotes the formation of zinc dendrite and induces dendrite growth through the “tip effect”, which significantly reduces the battery's cycling lifespan. Conversely, DMPII-modified LiI+I_2 electrodes show more uniform zinc ion deposition (Fig. S3b) at the anode interface compared to LiI+I_2-based electrodes (Fig. S3c). The latter displays a rough surface, indicating poor resistance to side reactions. Considering the inevitable diffusion of DMPII in the Zn-I_2 cells, the 0.03 M DMPII materials are added to the symmetric Zn//Cu cells with the electrolyte (0.5 M $ZnSO_4$ and Li_2SO_4 aqueous solution) to analyze the influence of DMPII materials on zinc anodes.[5] To ascertain the electrochemical performance of the DMPII additive, the plating/stripping experiments are performed in both symmetric and asymmetric Zn ion battery configurations.[4, 5, 7] The symmetric cells facilitated the assessment of Zn deposition and dissolution, while the asymmetric cells provided insights into the overall electrochemical stability and reversibility of the Zn ion cell system. The Coulombic efficiency of Zn//Cu cells of Zn with DMPII modification can stably cycle for 100 cycles with a high average Coulombic efficiency of 98 %, whereas the control pure Zn cell shows obvious fluctuations of Coulombic efficiency after 25

View Article Online
DOI: 10.1039/D4TA02558J

plating/stripping cycles (Fig. S4a). The corresponding overlapped voltage profiles of Zn with DMPII modification cell verify that the DMPII plays a crucial role in improving the reversibility and stability of the Zn electrode, where Zn with DMPII modification cell and pure Zn cell are 125 and 162 mV (Fig. S4b-c).[6, 7] The nucleation overpotential is the specific electrochemical potential at which the reduction of zinc ions initiates on the electrodes, which is observed while sweeping the potential from -0.2 V to 2.0 V in the CV curves of Zn//Ti cells. The potential is located at the crossover point A (crossover potential), and Zn ions start to be reduced on the electrode at point B, where nucleation overpotential is a potential disparity between A and B. The nucleation overpotential of Zn with DMPII modification, and pure Zn cells is 0.065, and 0.053 V, which the larger the nucleation overpotential indicates the smaller the radius of the nucleated Zn particles, leading to a dense and homogeneous deposition of Zn ions (Fig. S4d-e).[10, 11] Chronoamperometry (CA) measurements reveal the Zn^{2+} ion diffusion behavior on the surface of the Zn anode in the Zn//Zn cells,[28] which are performed at -150 mV. After approximately 100 s in the Zn//Zn cells, the Zn with DMPII modification cell stabilizes at approximately - 5 mA, which exposes a short two-dimensional (2D) diffusion of Zn ions. Instead, the pure Zn cell shows rapid decay in the current curve between 1 and 150 s, indicating a disordered diffusion process of Zn ions which correlates with the uneven nucleation and 3D dendritic growth (Fig. S4f).[6, 7, 29] In what follows, the long-term cycling stability of zinc anodes in electrolytes containing DMPII has been assessed using Zn//Zn symmetric cells. This investigation aims to evaluate the efficacy of DMPII as an additive in inhibiting dendrite formation, a critical factor in the safety of zinc-based cells. Under the current density of 2 mA/cm^2 and capacity of 2 mAh/cm^2, the cell employing a DMPII-based electrolyte demonstrates enhanced longevity, achieving a stable lifespan of up to 500 hours without any significant deviations in voltage, indicative of its superior performance and reliability in zinc-based energy storage systems (Fig. S5a-b).[4, 5] The following analysis, the electrochemical impedance spectroscopy (EIS) curves render sections as internal resistance of the electrolyte, interfacial resistance (R_S), and Warburg impedance.[24, 25] The alterations in interfacial resistance observed in Zn//Zn symmetric cells provide an indirect measure of the accumulation of electrochemically inert by-products on the surface of metallic zinc electrodes during the battery's cycling (Fig. S6a). These changes in impedance are indicative of the interfacial processes that occur as a result of the formation and deposition of such by-products, which can impact

View Article Online
DOI: 10.1039/D4TA02558J

the overall performance and stability of zinc-iodine cells. Cells modified with DMPII demonstrate the lowest charge transfer resistance among symmetric cells (Fig. S6b). This finding suggests that the incorporation of the DMPII-based electrolyte effectively mitigates the formation of electrochemically inert by-products during the zinc plating and stripping processes, thereby enhancing the electrochemical performance of zinc-iodine batteries.[4-7]

According to frontier molecular orbital theory, electron affinity, and electron donating capability are simulated by the density functional theory (DFT) calculations, which are respectively dependent on the energy levels of the lowest unoccupied molecular orbital (LUMO) and the highest occupied molecular orbital (HOMO).[38, 42-45] The I_2, I^-, I_3^-, DMP^+-I^-, and DMP^+-I_3^- have the LUMO energy level (-4.93, 17.09, 0.03, -0.839, and -3.06 eV, respectively), and the corresponding HOMO energy level are -7.50, -0.22, -2.68, -4.22, and -5.77 eV, respectively (Fig. 6a). The anchoring structure of DMP^+-I^- and DMP^+-I_3^- shows the similar LUMO-HOMO gap with that of I_3^-, which is 3.38 and 2.71 eV (2.65 eV for I_3^-).[18] Furthermore, the molecular configuration is very similar to each other, where the bond length of N-I is 0.380, and 0.377 nm for DMP^+-I^- and DMP^+-I_3^-, and the bond angle of N-I are 32.1^0, and 29.8^0 for DMP^+-I^- and DMP^+-I_3^-, respectively (Fig. 6b-c). Therefore, DMPII molecular can accelerate the coordination reaction of I^- and I_3^- to further prefer to form the large groups of DMP^+-I^-, and DMP^+-I_3^- structure, suppressing the shuttling effect of I_3^- and attribute to high Coulombic efficiency. More briefly, the N sites (Lewis acids) of DMPII molecular are capable of accepting an electron pair from a Lewis base (polyiodide ions) to form a Lewis adduct, which also is revealed by the Lewis acids and bases (Fig. 6d).[20] As such, the N sites of DMPII molecular facilitates the conversion of polyiodides and enhance the reaction kinetics in the Zn-I_2 batteries.

Conclusions

In summary, a facile in-situ strategy for constructing high-performance Zn-I_2 batteries is delivered by leveraging a commercially available DMPII activator. The composite cathodes significantly suppress the shuttle effect of triiodide and show a high specific capacity of 147 mAh/g, and ultralong cycling performance of over 20000 cycles is achieved with a capacity retention of 70 %. Notably, the N-functionalization in DMPII plays a pivotal role: electrostatic interactions between positively charged N^+

and negatively charged I_3^- significantly reduce triiodide diffusion, as confirmed by in-situ Raman, DFT calculations, and electrochemical analysis. The above-mentioned investigations reveal faster reaction kinetics and enhanced confinement within the DMPII-based cathodes during redox processes. Furthermore, this work provides the potential of commercially available functional materials through scientific investigation, paving the way for advancements in metal-iodine batteries.

Supporting Information

The Supporting Information is available free of charge at:…

Declaration of competing interest

The authors declare no conflict of interest.

Acknowledgments

This work was supported by the Science and Technology Development Fund (FDCT) of Macao S.A.R (0033/2023/ITP1, and 0022/2023/RIB1), the National Natural Science Foundation of China (61904080, and 22205101), the Cultivation Program for The Excellent Doctoral Dissertation of Nanjing Tech University, the Macau Young Scholars Program (AM2020005), Guangdong Basic and Applied Basic Research Foundation (2022A1515110994, and 2024A1515030228), and the High-Performance Computing Cluster (HPCC) of Information and Communication Technology Office (ICTO) at University of Macau.

Figures

View Article Online
DOI: 10.1039/D4TA02558J

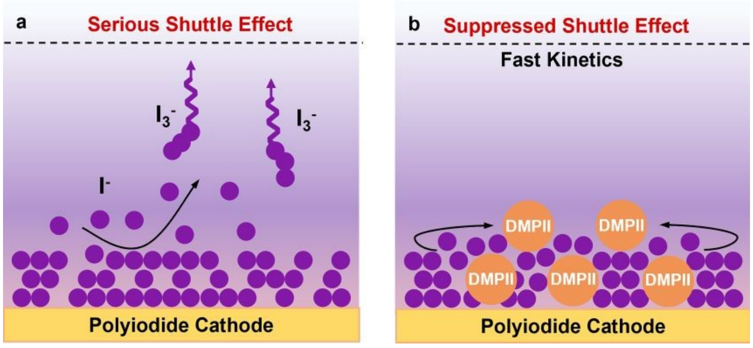

Fig. 1. Schematic illustration of polyiodide diffusion in the pure electrolyte (a) and DMPII molecule-based electrolyte (b).

View Article Online
DOI: 10.1039/D4TA02558J

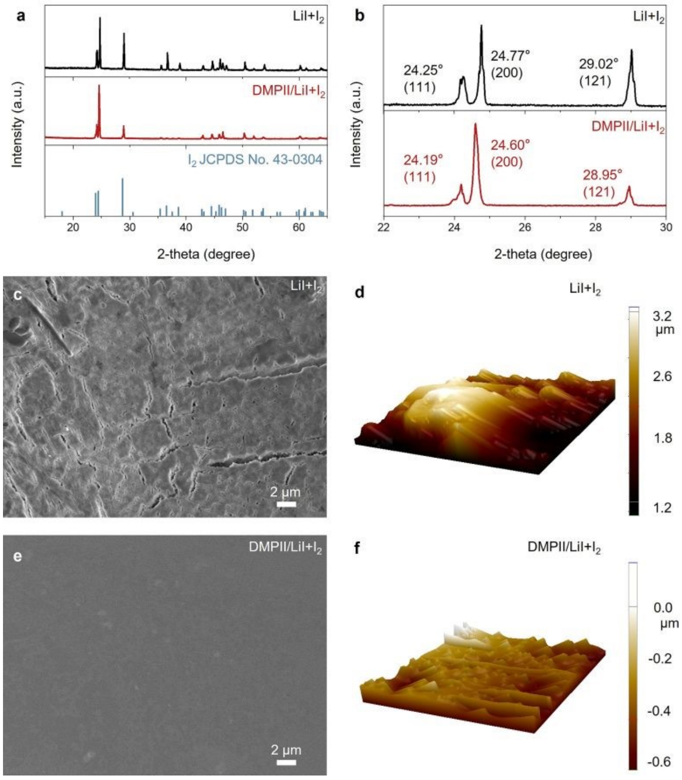

Fig. 2. XRD patterns (a) and magnified diffraction peaks (b) of pure LiI+I$_2$ catholyte and pure LiI+I$_2$ catholyte with DMPII. SEM, AFM images of pure catholyte (c, d), and pure catholyte with DMPII (e, f).

View Article Online
DOI: 10.1039/D4TA02558J

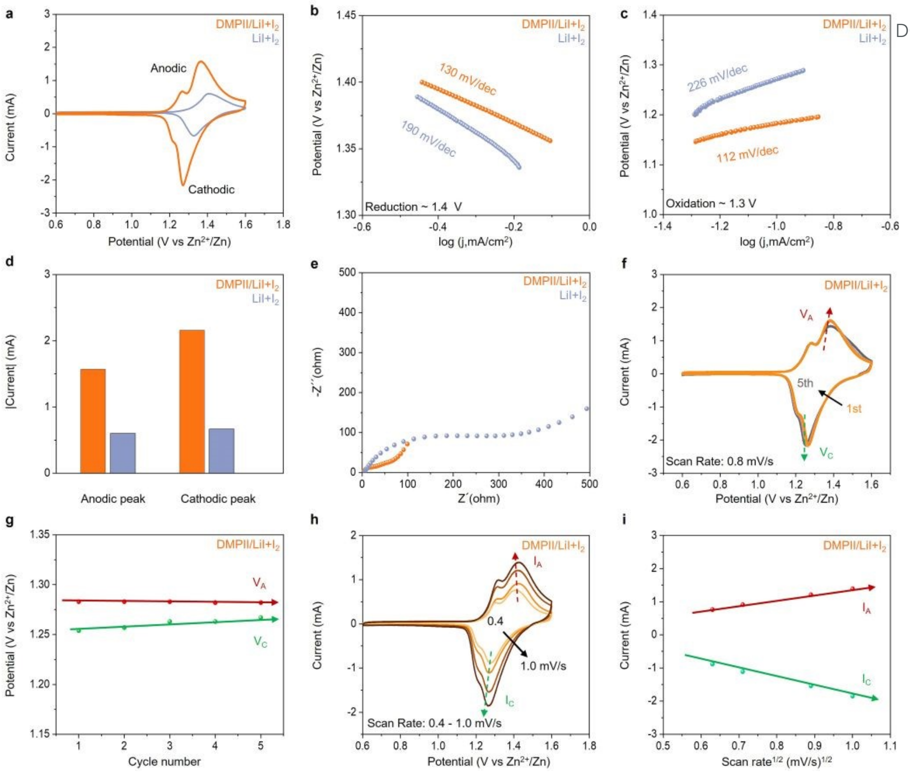

Fig. 3. The CV curves (a) of pure LiI+I_2 catholyte, LiI+I_2 catholyte with DMPII, and pure DMPII with the corresponding Tafel slopes (b, c) and peak current(d). Nyquist plots (e) of pure LiI+I_2 catholyte, and LiI+I_2 catholyte with DMPII. Stabilized CV curves (f) of the DMPII-based cell with the corresponding redox peak potentials (g), and the rated CV curves (h) of the DMPII-based cell with the corresponding redox peak of currents from the square root of the scan rate (i).

View Article Online
DOI: 10.1039/D4TA02558J

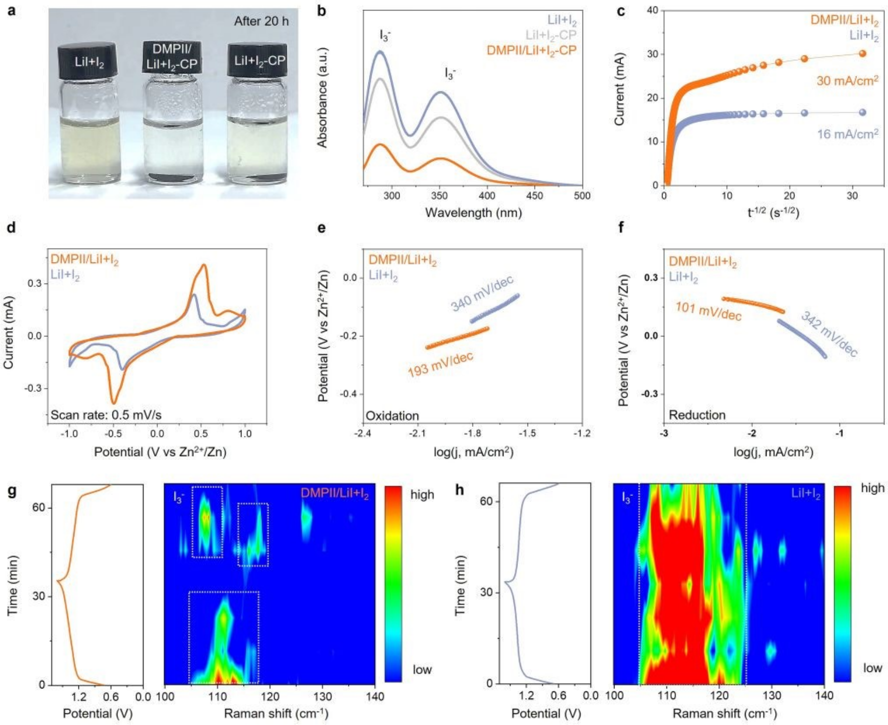

Fig. 4. The optical image (a), and UV-vis adsorption spectra (b) of pure $LiI+I_2$, DMPII/$LiI+I_2$-CP, and $LiI+I_2$-CP solutions. The Cottrell plots (c), CV curves (d), and the corresponding Tafel slopes (e-f) of the DMPII/$LiI+I_2$-CP and $LiI+I_2$-CP catholyte-based symmetric cells. *In situ* Raman spectra (g-h) showing charge/discharge of polyiodide conversion in DMPII/$LiI+I_2$-CP, and $LiI+I_2$-CP catholytes in the Zn-I_2 cells.

View Article Online
DOI: 10.1039/D4TA02558J

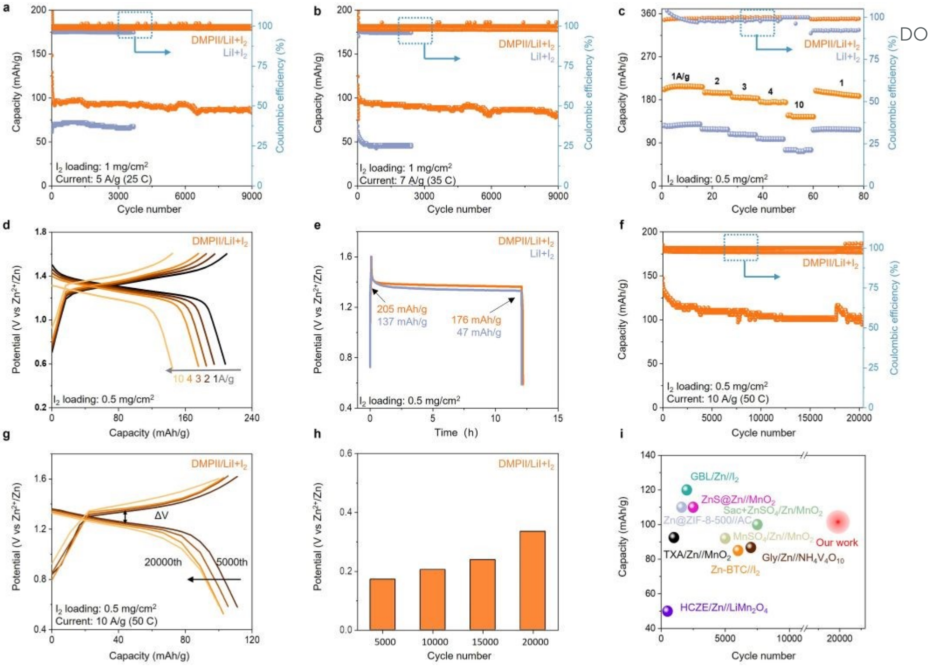

Fig. 5. Cycle stability (a, b) and rate performances (c) of Zn-I$_2$ cells using pure LiI+I$_2$ catholyte, and LiI+I$_2$ catholyte with DMPII, the corresponding charge-discharge curves (d), and self-discharge curves (e). The long-term cycling performance (f), the corresponding charge-discharge curves (g), and polarization potential (h) of Zn-I$_2$ cells using LiI+I$_2$ catholyte with DMPII. Comparison of cycle performances (i) with other similar Zn ion batteries (detailed description of abbreviation in Table S1).

View Article Online
DOI: 10.1039/D4TA02558J

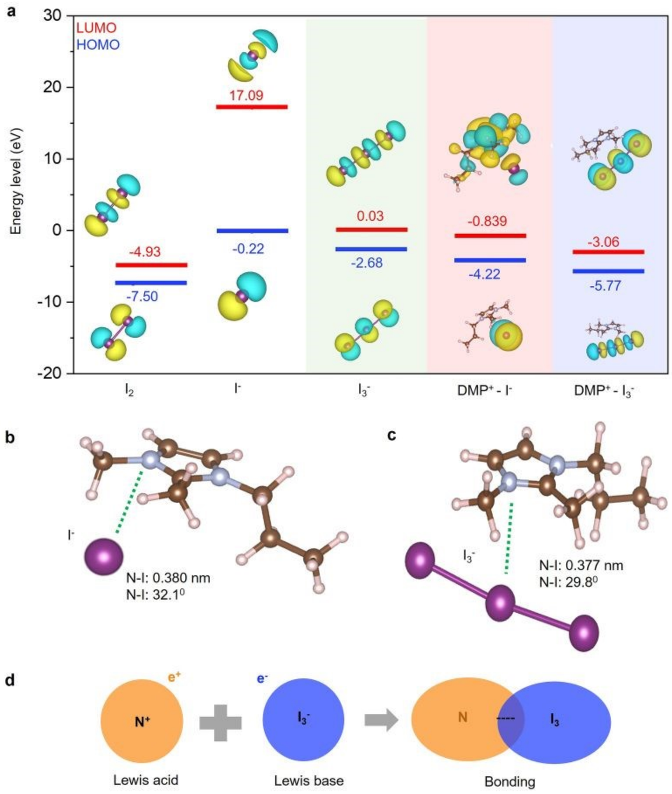

Fig. 6. LUMO-HOMO energy level diagram (a) of I_2, I^-, I_3^-, DMP-I^- and DMP-I_3^-. The cyan and yellow surfaces represent the orbital wavefunction in opposite directions. Confinement effect of I^- (b) and I_3^- (c) ions in DMP- molecule, and mechanisms of related intermolecular interactions (d).

View Article Online
DOI: 10.1039/D4TA02558J

References:

1. M. Han, D. Chen, Q. Lu and G. Fang, *Small*, 2023, 2310293.
2. H. Chen, X. Li, K. Fang, H. Wang, J. Ning and Y. Hu, *Adv. Energy Mater.*, 2023, **13**, 2302187.
3. J. Lin, Y. Yan, J. Qi and C. Zha, *Tungsten*, 2024, **6**, 269-277.
4. M. Wang, J. Ma, H. Zhang, L. Fu, X. Li and K. Lu, *Small*, 2024, **20**, 2307021.
5. J. Ma, M. Wang, H. Zhang, L. Fu, W. Zhang, B. Song, S. Lu, Q. Chen and K. Lu, *Mater. Today Energy*, 2022, **30**, 101146.
6. J. Ma, A. Azizi, E. Zhang, H. Zhang, A. Pan and K. Lu, *Chem. Sci.*, 2024, **15**, 4581-4589.
7. P. Jiang, Q. Du, C. Lei, C. Xu, T. Liu, X. He and X. Liang, *Chem. Sci.*, 2024, **15**, 3357-3364.
8. R. Wu, H. Xu, Y. Zhao, C. Zha, J. Deng, C. Zhang, G. Lu, T. Qin, W. Wang, Y. Yin, C. Zhu, L. Wang, G. Ouyang and W. Huang, *Energy Storage Mater.*, 2020, **32**, 216-224.
9. T. Liu, H. Wang, C. Lei, Y. Mao, H. Wang, X. He and X. Liang, *Energy Storage Mater.*, 2022, **53**, 544-551.
10. S. J. Zhang, J. Hao, H. Li, P. F. Zhang, Z. W. Yin, Y. Y. Li, B. Zhang, Z. Lin and S. Qiao, *Adv. Mater.*, 2022, **34**, 2201716.
11. X. Li, N. Li, Z. Huang, Z. Chen, G. Liang, Q. Yang, M. Li, Y. Zhao, L. Ma, B. Dong, Q. Huang, J. Fan and C. Zhi, *Adv. Mater.*, 2021, **33**, 2006897.
12. X. Jin, L. Song, C. Dai, Y. Xiao, Y. Han, X. Li, Y. Wang, J. Zhang, Y. Zhao, Z. Zhang, N. Chen, L. Jiang and L. Qu, *Adv. Mater.*, 2022, **34**, 2109450.
13. L. Yan, S. Zhang, Q. Kang, X. Meng, Z. Li, T. Liu, T. Ma and Z. Lin, *Energy Storage Mater.*, 2023, **54**, 339-365.
14. F. Yang, J. Long, J. A. Yuwono, H. Fei, Y. Fan, P. Li, J. Zou, J. Hao, S. Liu, G. Liang, Y. Lyu, X. Zheng, S. Zhao, K. Davey and Z. Guo, *Energy Environ. Sci.*, 2023, **16**, 4630-4640.
15. J. He, Y. Mu, B. Wu, F. Wu, R. Liao, H. Li, T. Zhao and L. Zeng, *Energy Environ. Sci.*, 2024, **17**, 323-331.
16. L. Ma, Y. Ying, S. Chen, Z. Huang, X. Li, H. Huang and C. Zhi, *Angew. Chem.Int. Ed.*, 2021, **133**, 3835-3842.
17. Y. Lyu, J. A. Yuwono, P. Wang, Y. Wang, F. Yang, S. Liu, S. Zhang, B. Wang, K. Davey, J. Mao and Z. Guo, *Angew. Chem.Int. Ed.*, 2023, **62**, e202303011.
18. P. Li, Y. Wang, Q. Xiong, Y. Hou, S. Yang, H. Cui, J. Zhu, X. Li, Y. Wang, R. Zhang, S. Zhang, X. Wang, X. Jin, S. Bai and C. Zhi, *Angew. Chem.Int. Ed.*, 2023, **135**, e202303292.
19. J. Wu, J. L. Yang, B. Zhang and H. J. Fan, *Adv. Energy Mater.*, 2023, 2302738.
20. S. Wang, Z. Huang, B. Tang, X. Li, X. Zhao, Z. Chen, C. Zhi and A. L. Rogach, *Adv. Energy Mater.*, 2023, **13**, 2300922.
21. G. Wang, Q. Yao, J. Dong, W. Ge, N. Wang, Z. Bai, J. Yang and S. Dou, *Adv. Energy Mater.*, 2023, 2303221.
22. Y. Du, R. Kang, H. Jin, W. Zhou, W. Zhang, H. Wang, J. Qin, J. Wan, G. Chen and J. Zhang, *Adv. Funct. Mater.*, 2023, **33**, 2304811.

View Article Online
DOI: 10.1039/D4TA02558J

23. M. Wang, J. Ma, H. Zhang, L. Fu, X. Li and K. Lu, *Small*, 2023, 2307021.
24. Y. Zou, T. Liu, Q. Du, Y. Li, H. Yi, X. Zhou, Z. Li, L. Gao, L. Zhang and X. Liang, *Nat. Commun.*, 2021, **12**, 170.
25. Z. Li, X. Wu, X. Yu, S. Zhou, Y. Qiao, H. Zhou and S.-G. Sun, *Nano Lett.*, 2022, **22**, 2538-2546.
26. T. Wei, Y. Ren, Y. Wang, L. e. Mo, Z. Li, H. Zhang, L. Hu and G. Cao, *ACS Nano*, 2023, **17**, 3765-3775.
27. K. Gao, S. Ju, S. Li, S. Zhang, J. Liu, T. Yang, J. Lv, W. Yu and Z. Zhang, *ACS Nano*, 2023, **17**, 18359-18371.
28. Q. Guo, H. Wang, X. Sun, Y. n. Yang, N. Chen and L. Qu, *ACS Materials Lett.*, 2022, **4**, 1872-1881.
29. H. Pan, B. Li, D. Mei, Z. Nie, Y. Shao, G. Li, X. S. Li, K. S. Han, K. T. Mueller and V. Sprenkle, *ACS Energy Lett.*, 2017, **2**, 2674-2680.
30. C. Zha, D. Wu, T. Zhang, J. Wu and H. Chen, *Energy Storage Mater.*, 2019, **17**, 118-125.
31. L. Zhang, M. Zhang, H. Guo, Z. Tian, L. Ge, G. He, J. Huang, J. Wang, T. Liu, I. P. Parkin and F. Lai, *Adv. Sci.*, 2022, **9**, 2105598.
32. B. Liu, H. Chen, J. Cao, X. Chen, J. Xie, Y. Shu, F. Yan, W. Huang and T. Qin, *Adv. Funct. Mater.*, 2023, 2310828.
33. Y. Zhao, L. Zhang, J. Xiang, X. Chen, C. Zhu, K. Wang, J. Li, H. Ma, X. Song and L. Wang, *Mater. Today Phys.*, 2023, **32**, 101029.
34. C. Zha, S. Wang, C. Liu, Y. Zhao, B. He, C. Lyu, J. Li, S. Ji, S. Chen and K. San Hui, *Energy Storage Mater.*, 2022, **47**, 79-86.
35. Y. Yang, S. Liang, B. Lu and J. Zhou, *Energy Environ. Sci.*, 2022, **15**, 1192-1200.
36. Y. Zhao, Z. Zhang, R. Wu, C. Lyu, X. Zhao, H. Xu, J. Xiang, C. Zha, G. Ouyang and L. Wang, *Mater. Today Energy*, 2021, **21**, 100793.
37. Y. Zhao, D. Wu, T. Tang, C. Lyu, J. Li, S. Ji, C. Yuan, K. San Hui, C. Zha and K. N. Hui, *J. Mater. Chem. A*, 2022, **10**, 4015-4023.
38. C. Zha, F. Yang, J. Zhang, T. Zhang, S. Dong and H. Chen, *J. Mater. Chem. A*, 2018, **6**, 16574-16582.
39. H. Ye, J. Sun, S. Zhang, H. Lin, T. Zhang, Q. Yao and J. Y. Lee, *ACS Nano*, 2019, **13**, 14208-14216.
40. C. Zha, X. Zhu, J. Deng, Y. Zhou, Y. Li, J. Chen, P. Ding, Y. Hu, Y. Li and H. Chen, *Energy Storage Mater.*, 2020, **26**, 40-45.
41. Y. Kato, S. Hori, T. Saito, K. Suzuki, M. Hirayama, A. Mitsui, M. Yonemura, H. Iba and R. Kanno, *Nat. Energy*, 2016, **1**, 1-7.
42. P. E. Blöchl, *Phys. Rev. B*, 1994, **50**, 17953.
43. G. Kresse and J. Furthmüller, *Phys. Rev. B*, 1996, **54**, 11169.
44. J. P. Perdew, K. Burke and M. Ernzerhof, *Phys. Rev. Lett.*, 1996, **77**, 3865.
45. C. Zha, X. Gu, D. Wu and H. Chen, *J. Mater. Chem. A*, 2019, **7**, 6431-6438.